ACS OMEGA

Open Access

http://pubs.acs.org/journal/acsodf

Article

Controlled Calcium Oxalate Crystals Obtained by Electrocrystallization on Electrospun Polycaprolactone Fibers Loaded with Zarzaparrilla (*Herreria stellata*)

Andrónico Neira-Carrillo,* Tatiana Zegers Arce, and Mehrdad Yazdani-Pedram

Cite This: *ACS Omega* 2024, 9, 17045−17053

Read Online

ACCESS | Metrics & More | Article Recommendations | Supporting Information

ABSTRACT: Calcium oxalate (CaOx) is known to grow on organic matrices and is often associated with the formation of kidney stones. Therefore, it is crucial to understand the nucleation and growth mechanisms. This study investigates the role of electrospun polycaprolactone (PCL)-loaded zarzaparrilla (ZP) (*Herreria stellata*) in the electrocrystallization (EC) of CaOx. Electrospinning (ES) was used to prepare PCL meshes with random (R) and aligned (A) fiber orientations. CaOx particles were grown directly on conductive tin indium oxide (ITO) glass modified with electrospun ZP-loaded PCL meshes by EC. The CaOx crystals after EC were measured by chronopotentiometry (CP), optical microscopy (OM), scanning electron microscopy (SEM), and X-ray diffraction (XRD), which showed that the ZP additive and PCL fiber orientations are key factors for CaOx nucleation.

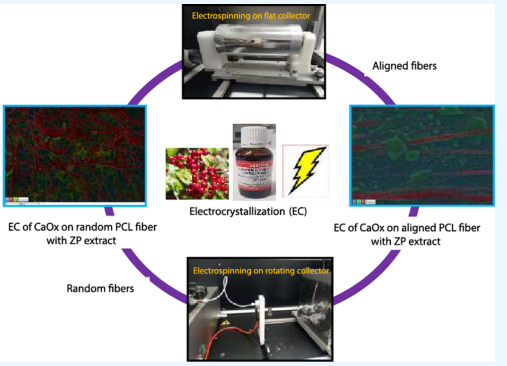

1. INTRODUCTION

Biomineralization is a process used by living organisms to produce biogenic minerals. This process involves the close association of inorganic and organic components under mild and environmentally friendly conditions.[1,2] The organic component of biominerals controls the nucleation, crystal growth, morphology, orientation, and spatial confinement of mineral crystal structures.[3−5]

Calcium oxalate (CaOx) is the most common oxalate mineral found in living organisms and the environment. CaOx has several functions in living organisms and can take on different crystal shapes and sizes. It occurs in three hydrated forms, such as monohydrated (COM or whewellite), dihydrated (COD or weddellite), or trihydrated (COT or caoxite). COM is commonly associated with kidney stones (urolithiasis) in mammals but can also occur in healthy individuals. In fact, the COM and COD forms are the main constituents of the majority of urinary stones.[6,7]

There is a growing interest in studying the crystallization of CaOx in vitro and in vivo using solid templates, additives, and herbal plants, to elucidate the mechanism involved in urolithiasis disease and to fabricate hierarchical hybrid materials.[8−16] Thus, citrate, for example, can affect the crystallization process by interacting electrostatically with certain phases of CaOx crystals. This interaction prevents the pathological formation of COM crystals, which are considered the primary constituent of the critical process in the pathogenesis of kidney stones.[9,17−19] The molecular recognition at the interface between the organic and inorganic components of CaOx is of paramount importance. However, the stabilization of a specific hydrated form of CaOx in vitro is not fully understood.

Accordingly, the authors have reported on the use of electrospun polycaprolactone (PCL) fibers as a platform to study the in vitro formation of CaOx by the electrocrystallization (EC) method. EC is a process in which crystals are grown on a glassy substrate by applying an electric field.[17]

In this context, zarzaparrilla (*Herreria stellata*) (ZP)-loaded PCL fibers were used as a template to form CaOx on the surface of the fibers. ZP is a plant traditionally used for its medicinal properties, including its anti-inflammatory and antioxidant effects. By incorporation of ZP on electrospun polymer mesh (EPM) during the EC, the growth of CaOx can be controlled by the presence of ZP in the EPM matrix. In vitro antiurolithic effect of the natural extract of Terminalia arjunia on CaOx has been explored by using an aqueous extract of *Terminalia arjunia* to study the nucleation, aggregation, and growth effects associated with its antilithiatic activity.[20] ZP-loaded solid fibrillary matrices as urolithiasis modulators represent an interesting approach to study their role in the prevention of kidney stones through in vitro CaOx

Received: November 3, 2023
Revised: March 7, 2024
Accepted: March 22, 2024
Published: April 6, 2024

crystallization in a one-step process followed by chronopotentiometry (CP) technique.

In fact, the effect of EPM using biopolymer on mineralization of CaOx and calcium carbonate has been reported by us.[21,22] The application of EPM has been studied due to its ability to produce micro and nanofiber with high specific surface area.[23] Anionic chemical moieties can be added to the surface of the EPM, where the surface area of the EPM provides an effective interaction with Ca^{2+} ions, inducing local ion concentration or anchoring molecular sites.

Given the above evidence that the EPM plays a pivotal role in CaOx crystallization, random (R-PCL) and aligned (A-PCL) fibers loaded with ZP were fabricated using an organic template on the EC of CaOx. We also report the modifying effect of ZP on CaOx crystal growth, COD stabilization, and inhibition of the pathological COM form.

2. EXPERIMENTAL SECTION

2.1. Preparation of Electrospun PCL Fibers. Electrospun poly(ε-caprolactone) (EPM) fibers, both random (R-PCL) and aligned (A-PCL), were directly deposited onto indium tin oxide (ITO) glass pieces to serve as templates for the EC of CaOx. EPM fibers were prepared from a mixture of acetone and ethyl acetate (3:1 v/v) in a solution of 18% PCL (Mw 80 000, Sigma-Aldrich). PCL solutions were stirred at 40 °C until completely dissolved. They were then left to stand overnight at room temperature and transferred to a 10-mL Nipro luer-lock syringe. The production of PCL-EPM was carried out on an eStretching LE-10 Fluidnatek instrument. Briefly, pieces of ITO glass were bonded to the rotating drum and flat plate collectors and then used as the working electrode for the EC process (Figure 1). R-PCL and A-PCL fibers were prepared using a flat 30 × 30 at 15 cm and a rotating 10-cm diameter at 2000 rpm metal collectors. The 9.5 kV voltage and 1000 μL/h flow rate solution were used for the preparation of the PCL-EPM. PCL fiber deposition was performed on Corning ITO glass (25 × 25 mm; 1.1 mm thick) supplied by Delta Technologies (Dallas, Texas, USA) using 10 × 25 mm ITO pieces. All commercially available ITO glasses have a sheet surface resistivity in the range of 5−15 Ω/sq. For the preparation of working solutions and the CaOx EC method, high-purity water (Milli-Q quality and resistivity >18.2 MΩ cm^{-1}) was used from a LabostarTM TWF water purification system (Evoqua Water Technologies LLC, Warrendale, PA, USA).

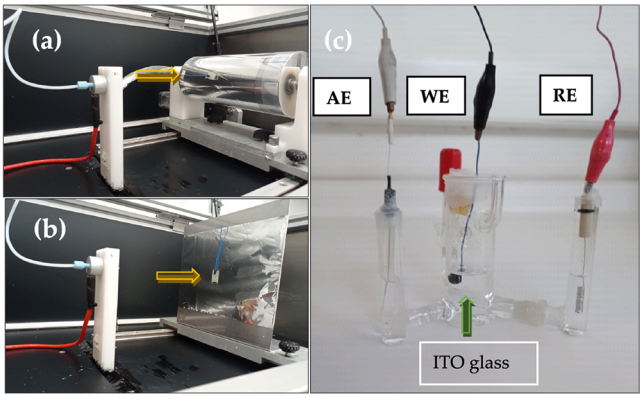

Figure 1. Optical images showing the PCL-EPM on pieces of ITO glass used as templates on the EC of CaOx glued to (a) a rotating drum (rotation speed of 1800 rpm, clockwise), (b) a flat plate collector, and (c) a glass vial utilized in the in vitro EC of CaOx. Orange and green arrows indicate the electrode cable connected to ITO on both collectors and inmersed in the EC soltions, respectively. The white, black, and red electrode cables correspond to the auxiliary (AE), working (WE), and reference (RE) electrodes.

2.2. Electrocrystallization of CaOx. The CaOx EC, containing either R-PCL or A-PCL fibers loaded with ZP on ITO glass, was carried out using a galvanostat/potentiostat (BASi Epsilon) instrument (West Lafayette, Indiana, USA) as previously reported.[17,21,24] Briefly, pieces of ITO glass attached to the surfaces of rotating and flat plate collectors were used to directly fabricate PCL-EPM by using the ES method. They were then used as templates in the presence of ZP on the EC of CaOx. All the EC assays were done in a glass electrochemical cell. The ITO glasses were submerged in solutions of calcium nitrate, ethylenediaminetetraacetic acid (EDTA), and sodium oxalate solutions at pH of 10.5. The EC of the CaOx process was achieved using 9 mA for 60 min, and the chronopotentiometry was registered with a 2 s recording interval of sampling. The CaOx crystals were formed during the EC due to the strong chelating properties of EDTA to Ca ions, forming a stable complex in an alkaline pH medium. When an electric potential is applied, water undergoes electrolysis, which generates free O_2 and protons at the ITO glass surface. This resulted in a pH decrease and destabilization of the Ca-EDTA complex.[18] Consequently, free Ca^{2+} ions react with oxalate ions to form CaOx of the WE on the surface of the ITO substrate. The deposition of CaOx on the ITO increases the resistance to current flow, leading to an increase in the recorded voltage during the EC experiment.

2.3. Characterization of PCL−EPM and CaOx. The CaOx particles formed on the ITO glass were analyzed by Fourier transform infrared spectroscopy (FTIR/ATR) using an Interspec 200-X instrument (Interspectrum OU, Toravere, Estonia). The CaOx and PCL-EPM morphologies were analyzed by optical microscopy (OM) and scanning electron microscopy (SEM) using the LAZ morphometric program (Image Pro-Plus, Media Cybernetics, Melville, NY, USA) on Nikon Eclipse E400 and JEOL JSM-IT300LV (JEOL USA Inc., Peabody, Massachusetts, USA) microscopes, respectively. For the SEM analysis, the samples were coated with 20 nm of gold by using the Denton Vacuum Desk V sputtering system in an argon atmosphere to ensure electrical conductivity. The SEM images were acquired by using a 20 kV accelerating voltage. X-ray diffraction (RXD) of PCL−EPM samples were performed using a Siemens D-5000X X-ray diffractometer with CuKα radiation (graphite monochromator) and an ENRAF Nonius FR 590 X-ray generator (PXRD) (Siemens, Munich, Germany). XRD spectra of CaOx crystals were obtained using CuKα radiation (40 kV) with a step scan of 0.2° and the geometric Bragg−Brentano (θ−θ) scanning mode with an angle (2θ) ranging from 5° to 60°. The DiffracPlus program was utilized for data control.

2.4. Statistical Analysis. All results are expressed as the mean ± standard deviation (SD). One-way analysis of variance (ANOVA) with significance based on $p < 0.05$ was conducted using differences between experimental groups in the Minitab 19 program. All the EC assays were performed in triplicate.

3. RESULTS AND DISCUSSION

3.1. Chronopotentiometry (CP). Figure 2 shows the CP behavior of the CaOx EC on the bare ITO (control, Figure 2a)

https://doi.org/10.1021/acsomega.3c08736
ACS Omega 2024, 9, 17045−17053

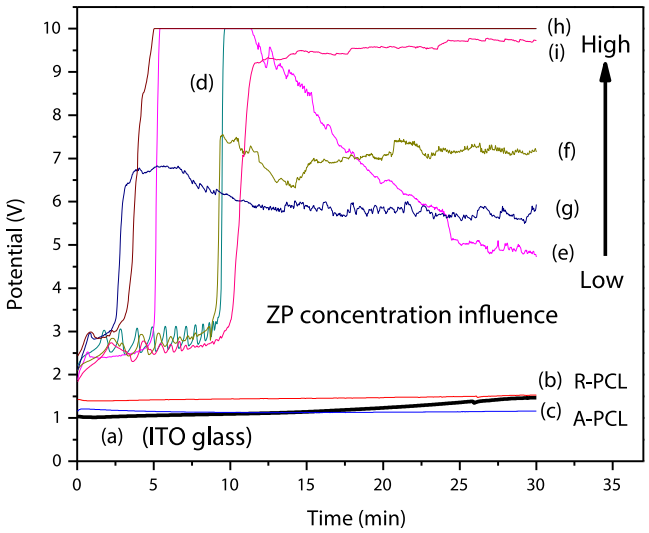

Figure 2. Chronopotentiometry of the EC of CaOx on ITO in the presence of PCL fibers and ZP using three concentrations of ZP for 30 min: (a) control (bare ITO), (b) R-PCL, (c) A-PCL, (d) A-PCL with 1 mg/L of ZP, (e) R-PCL with 1 mg/L of ZP, (f) A-PCL with 1 g/L of ZP, (g) R-PCL with 1 g/L of ZP, (h) A-PCL with 5 g/L of ZP, and (i) R-PCL with 5 g/L of ZP.

and in the presence of PCL-EPM (R-PCL Figure 2b and A-PCL Figure 2c). We observe that the potential (V) carried out on ITO (control) and on ITO with PCL-EPM (Figure 2a,b) without ZP was very similar during the CaOx EC, reaching a potential of 1.0 V. However, when the EC was performed using PCL-EPM with ZP additive at different concentrations, the potential (V) value increased to higher recorded values from mg/L (Figure 2d–e) to g/L (Figure 2f,i) concentrations, where the EC voltage started at 2.5 V and its potential (V) changed, reaching values in the range of 4–10 V at the end of the EC experiment. The chronopotentiometric curves obtained using PCL-EPM exhibited a significant increase in the potential (V). The onset potential values varied depending on the EC assay times and the type of PCL mesh utilized. Longer times were observed for higher ZP concentrations. In general, higher concentrations of the ZP additive resulted in a kinetically promoting effect on the CaOx mineral. We noticed that the CaOx particles formed on the ITO surface are not conductive materials. Therefore, their local presence reduces the active area of the electrode. Thus, the CaOx forms a barrier for oxygen diffusion and in this way the total cathodic current decreases, which can be followed by fluctuations of the potential (V).[25] The registered current can be analyzed during the time of the CaOx EC experiments. The deposited CaOx crystals can be registered when the WE surface is covered.

3.2. Optical (OM) and Scanning Electron Microscopy (SEM). The OM initially revealed the presence of CaOx on the A-PCL and R-PCL fibers on the ITO glass (control), on the ITO coated with only PCL-EPM, and on the ITO coated with PCL-EPM in the presence of ZP at various concentrations. See Figures S1 and S2. Although the OM technique has limited resolution, it was able to clearly distinguish the PCL-EPM arrangement, crystal morphologies, and crystal sizes of CaOx associated with both PCL-EPM fiber orientations and concentrations of ZP. Figure S1a–c shows the formation of CaOx crystals by in vitro EC on ITO without PCL fibers (control, Figure S1a), on ITO with A-PCL fibers (Figure S1b), and on ITO with R-PCL (Figure S1c), respectively. Figure S2 shows the CaOx formed on the ITO with PCL-EPM using A-PCL (Figure S2a–c) and R-PCL (Figure S2d–f) at concentrations of 1, 1, and 5 g/L of ZP.

On the other hand, the SEM analysis (Figure 3) enabled us to observe in more detail the morphology of the CaOx during

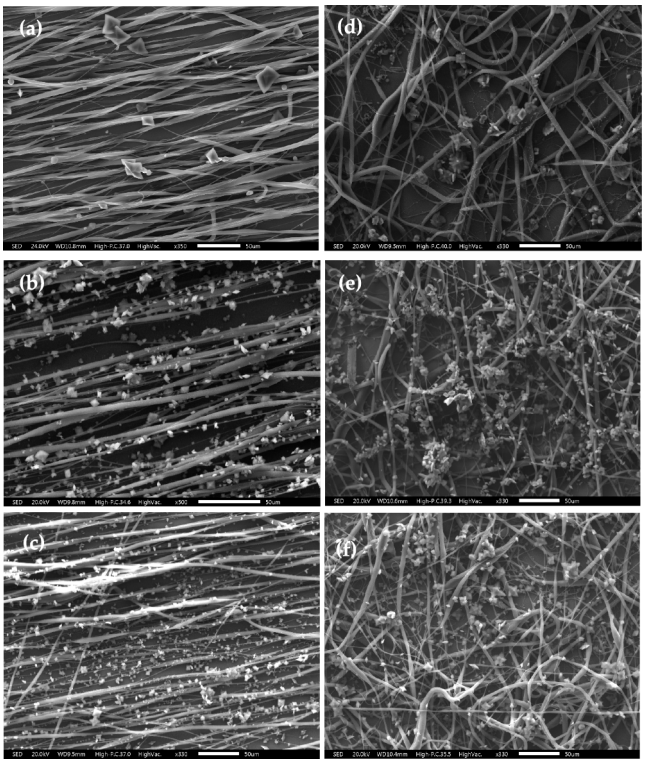

Figure 3. SEM images of CaOx crystals after EC on ITO in the presence of PCL fibers: (a) A-PCL with 1 mg/L ZP, (b) A-PCL with 1 g/L ZP, (c) A-PCL with 5 g/L ZP, (d) R-PCL with 1 mg/L ZP, (e) R-PCL with 1 g/L ZP, and (f) R-PCL with 5 g/L ZP.

the EC essays obtained with PCL-EPM loaded with ZP using A-PCL (Figure 3a–c) and R-PCL (Figure 3d,g) fibers, respectively. SEM images were consistent with the OM observations, where CaOx formed on ITO and both PCL-EMP fibers displayed differences in size and shape. A reduction in the number and size of CaOx crystals was observed with lower concentrations of ZP additives on both PCL meshes compared to control experiments when comparing the EC assay using ZP at different concentrations in both fibrillar matrices. The crystal size of the CaOx varied from 5 to 20 μm, with flower-like COD crystals of around 20 μm, and a few irregular circular crystals were observed (Figure 3a,d). When A-PCL fibers were used, spherical CaOx crystals were found to be more abundant at lower ZP concentrations.

In general, we found that the PCL-EMP fibers did not interfere with the formation of CaOx on the PCL-EPM matrices. In fact, Figure 3 indicates that the CaOx crystals obtained on A-PCL and R-PCL fibers with ZP are mainly distributed on the PCL fiber meshes, acting as a nucleation guide support.

We also performed SEM-EDS microanalysis of the resultant CaOx (Figure 4). Here, Figure 4a–c displays the elemental composition of the CaOx crystals, including calcium (Ca), carbon (C), and oxygen (O) atoms. We note that, due to the sensitivity and penetrability of the X-ray detector, the elements

https://doi.org/10.1021/acsomega.3c08736
ACS Omega 2024, 9, 17045–17053

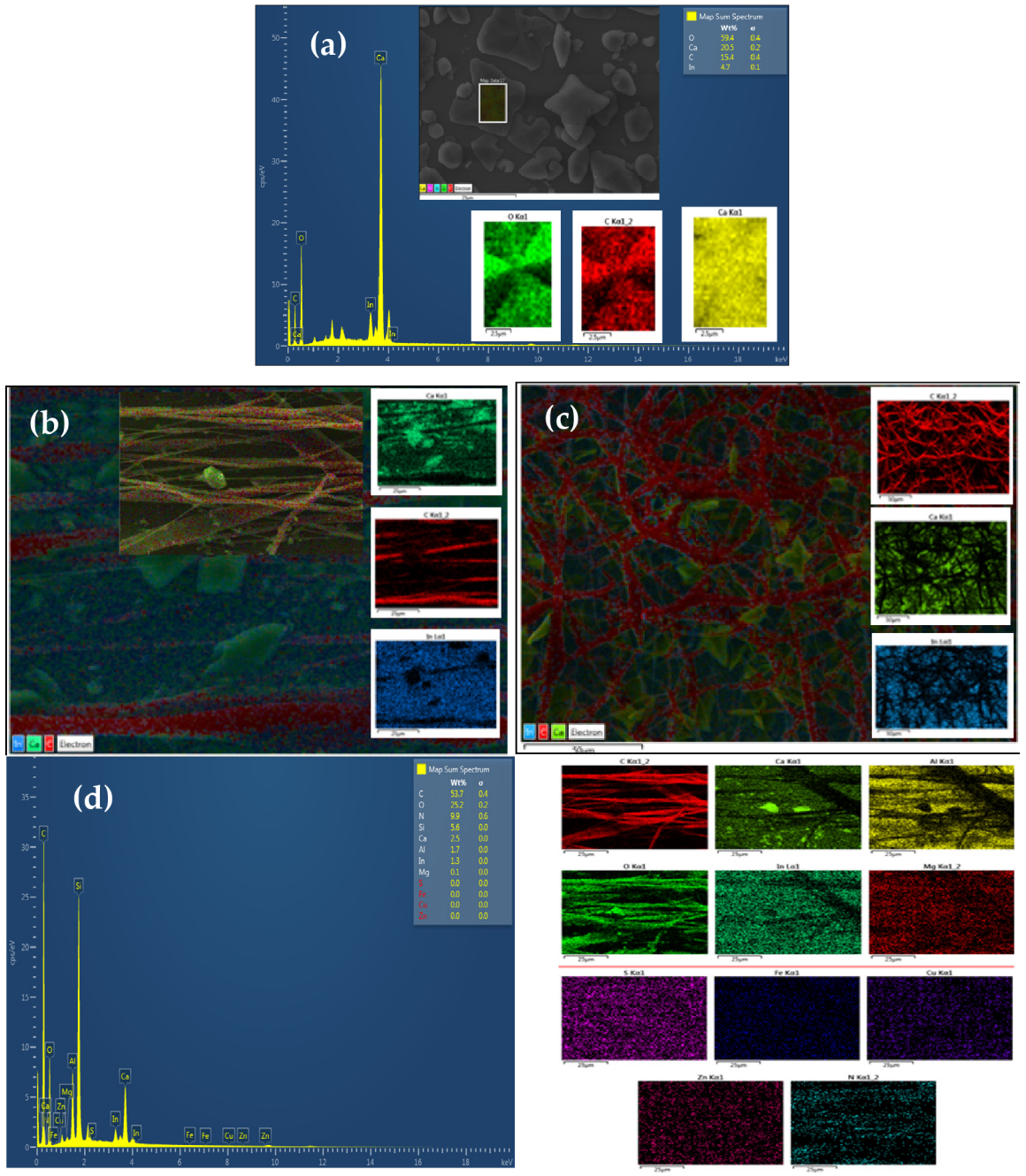

Figure 4. SEM-EDS analysis of CaOx crystals after EC on ITO in the presence of PCL fibers and ZP: (a) control (without PCL fibers), (b) A-PCL, (c) R-PCL, and (d) A-PCL with 1 g/L of ZP.

indium (In), aluminum (Al), and silicon (Si) from the ITO glass were detected, as well.

On the other hand, when the ZP additive was used at 1g/L ZP on the A-PCL fiber during the CaOx EC assays (Figure 4d), a wide range of elements were identified, such as magnesium (Mg), silicon (Si), aluminum (Al), sulfur (S), iron (Fe), copper (Cu), and zinc (Zn), which are considered typical elements for ZP.[26,27] It is worth mentioning that although the microanalysis identified certain elements, they could not be quantified due to low concentrations in the ZP additive.

3.3. X-Ray Diffraction (XRD). XRD analysis was conducted to demonstrate the CaOx phases obtained on the ITO glass during all CaOx EC using PCL-EPM with A-PCL (Figure 5a–c) and R-PCL fibers (Figure 5d–f). The XRD pattern of CaOx obtained on the ITO without PCL fibers (control) and on the PCL-EPM without ZP can be seen in Figure S3, where the crystallographic peaks corresponding to ITO, A-PCL, and R-PCL fibers are clearly distinguished. In order to identify the crystallographic signals for the hydration state of the CaOx phases, the COM phase (JCPDS card numbers 20−231) and the COD phase (JCPDS card number 17−541) were utilized.

The XRD patterns of CaOx crystals obtained on the ITO with A-PCL (Figure 5a–c) and R-PCL (Figure 5d–f) showed the phases of COD and COM at low ZP additive concentration. The crystallographic signals exhibited a decline at higher ZP concentrations (Figure 5c,f), indicating a COD phase predominance in Figure 5f. Additional peaks attributed

https://doi.org/10.1021/acsomega.3c08736
ACS Omega 2024, 9, 17045−17053

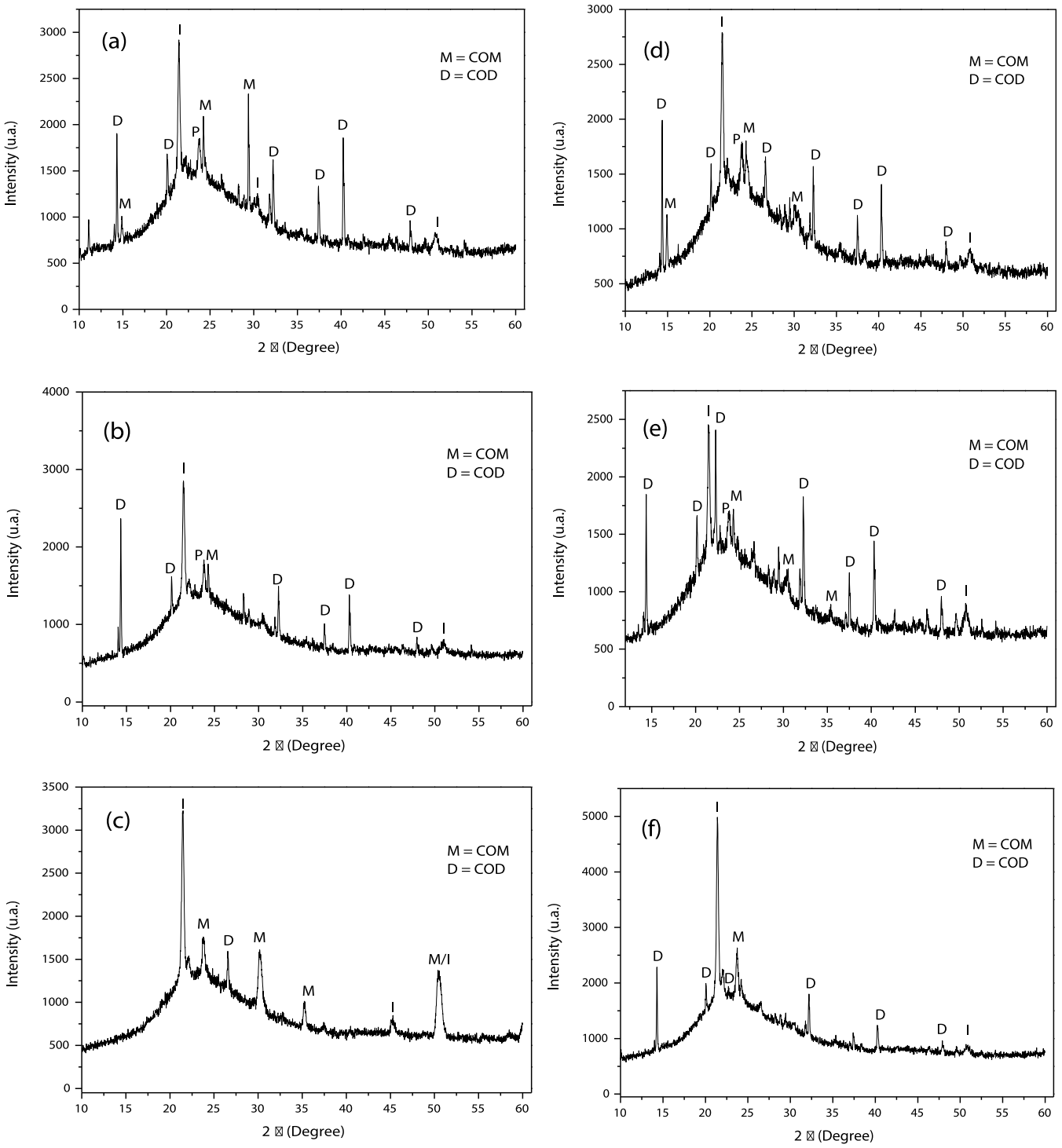

Figure 5. XRD of CaOx after EC obtained on ITO in the presence of PCL fibers and ZP additive: (a) A-PCL with 1 mg/L ZP, (b) A-PCL with 1 g/L ZP, (c) A-PCL with 5 g/L ZP, (d) R-PCL with 1 mg/L ZP, (e) R-PCL with 1 g/L ZP, and (f) R-PCL.

to the ITO substrate were consistently recorded and confirmed at (2 theta degree) 2θ = 21.4°, 30.3°, 45.5°, and 50.7° in every EC assay, as shown in Figure S3.

The COM phase exhibits crystallographic peaks at 2θ = 14.9°, 24.3°, 29,4°, 35.5°, and 37.7°, which correspond to the (hkl) indices of (−101), (020), (002), (301), and (311), respectively. Other peaks at 2θ = 14° (D), 20.1° (D), 22.7° (D), 23.8° (M), 24.3° (M), 32.2° (D), 37.4° (D), and 47.9° (D) correspond to planes (200), (211), (310), (−211), (020), (411), (103), and (413).

The XRD results suggest that the presence of ZP as an additive on the R-PCL and A-PCL meshes can modulate CaOx crystallization and promote the formation of COD crystals. When the CaOx EC experiments were carried out with PCL-EPM at higher ZP concentrations, most crystallographic peaks corresponding to COM showed lower intensity signals. Astoundingly, the peak at 2θ = 14.9° related to the pathogenic (−101) plane of the COM phase disappeared when using both PCL meshes, i.e., A-PCL at a concentration of 1 mg/L (Figure 5b,c) and R-PCL at a concentration of 1 g/L (Figure 5e,f) of

https://doi.org/10.1021/acsomega.3c08736
ACS Omega 2024, 9, 17045−17053

ZP. Surprisingly, our XRD results also showed that the XRD patterns of CaOx on the ITO containing R-PCL with 5 g/L of ZP belong to COD (Figure 5f). Additionally, polymer PCL signals (P) for electrospun PCL fibers were not detected.

To determine the total number of CaOx crystals (N), the number of CaOx crystals/mm^2, the sample size (n) as the selected number of crystals for all measurements, the average number of crystal sizes ($\bar{x}$), and the 95% confidence interval, the Minitab 19 program was used (Table S1). The confidence interval of the meshes was determined according to the type and orientation of the PCL fibers and the concentration of ZP. Analysis of the mean crystal size using the normality test (AndersonDarling) and the test for equality of variances (Bonferroni−Levene) indicated a non-normal distribution (Figure S4), and heteroscedasticity due to the variance of the errors was not constant (Figure S5).

Considering the experimental condition of the in vitro EC method, all samples are independent, and due to the non-normality, heteroscedasticity, and independence of the data, the determination of the difference between the mean crystal sizes was done by the Welch's test. Once the statistical difference was confirmed, the pairs of comparisons were carried out using the Games−Howell method (Figure S6). The confidence interval estimation and the determination of Games−Howell pairwise comparisons between all EC assays for CaOx are summarized in Tables 1−6 .

Table 1. Games−Howell Pairwise Comparison between the Negative Control Assays Using A-PCL Meshes on the CaOx EC with Three Concentrations of ZP

sample	n	$\bar{x}$	grouping	
ZP-A 1 mg/L	46	**8,644**	A	
CN-A	108	**7,933**	A	
ZP-A 1 g/L	220	*3,973*		B
ZP-A 5 g/L	272	*3,898*		B

The results of the smallest and largest mean values are shown in italics and bold, respectively. Medians that do not share a letter indicate that they are significantly different.

The statistical difference in the average number of crystals ($\bar{x}$) between the control test (CN-A) and ZP-A at 1 mg/L with the two highest ZP concentrations used in the CaOx EC experiments was shown by the Games−Howell test. Then, the effect of ZP on the variation of the average size of the crystals was demonstrated with smaller crystals when the EC was carried out with ZP at 1 and 5 g/L. Also, crystals with the largest average size were obtained with ZP at 1 mg/L. The crystals obtained with the A-PCL mesh without ZP showed the second largest size value.

The results of the smallest and largest mean values are shown in italics and bold, respectively. Medians that do not share a letter indicate that they are significantly different.

The Games−Howell test also showed a statistical difference in the n values obtained between the control assay (CN-R) with all the CaOx EC assays using ZP and the ZP lowest concentration of 1 mg/L, and the two highest ZP concentrations of 1 and 5 g/L. The effect of ZP on the variation of n was demonstrated by obtaining smaller CaOx crystals when ZP was used at a concentration of 1 mg/L in the EC and the largest average size of crystals when the EC was carried out with R-PCL without ZP.

The analysis of the intergroup pairwise comparisons between negative control using A-PCL (Table 1) and R-PCL (Table 2) meshes allows a quantitative estimation of the effect

Table 2. Games−Howell Pairwise Comparison between the Negative Control Assays Using R-PCL Meshes on the CaOx EC with Three Concentrations of ZP

sample	n	$\bar{x}$	grouping		
CN-R	38	**15,70**	A		
ZP-R 1 g/L	227	6,770		B	
ZP-R 5 g/L	199	6,193		B	
ZP-R 1 mg/L	148	*4,414*			C

of the ZP additive at its different concentrations and type of mesh in the EC experiments, considering the evaluation of one factor at a time in the analysis of the results. On the other hand, when making pairwise comparisons within groups (Tables 3 and 4), it is possible to evaluate simultaneously the effect of the ZP additive at the three concentrations depending on the PCL mesh and the crystals obtained in the EC assays.

Table 3. Games−Howell Pairwise Comparison between the Negative Control Assays Using A-PCL Meshes and Their CaOx EC with Three Concentrations of ZP

sample	n	$\bar{x}$	grouping		
ZP-A 1 mg/L	46	**8,644**		B	
CN-A	108	**7,933**		B	
ZP-A 1 g/L	220	*3,973*			C
ZP-A 5 g/L	272	*3,898*			C

Table 4. Games−Howell Pairwise Comparison between the Negative Control Assays Using R-PCL Meshes and Their CaOx EC with Three Concentrations of ZP

sample	n	$\bar{x}$	grouping		
CN-R	38	**15.70**	A		
ZP-R 1 g/L	227	6,770		C	
ZP-R 5 g/L	199	6,193		C	
ZP-R 1 mg/L	148	*4,414*			D

The results of the smallest and largest mean values are shown in italics and bold, respectively. Medians that do not share a letter indicate that they are significantly different.

The Games−Howell test showed that there was a statistical difference in the nanovalues obtained between ZP-A at 1 mg/L and CN-A with the two highest ZP concentrations of 1 and 5 g/L, but there was no statistical difference between the two highest ZP concentrations. In addition, the crystals with ZP at 1 and 5 g/L appeared to have a lower n value compared to that of CN-A and ZP at 1 mg/L. This indicates that the largest average crystal size in the EC assays was obtained with ZP-A at 1 mg/L. Thus, the effect of increasing ZP concentration was significant under the experimental conditions.

The results of the smallest and largest mean values are shown in italics and bold, respectively. Medians that do not share a letter indicate that they are significantly different.

The Games−Howell test showed that there was a statistical difference in the values of n between the control experiment (CN-R) with ZP-R at the three concentrations mentioned above used in the EC. It is observed that there was a statistical

https://doi.org/10.1021/acsomega.3c08736
ACS Omega 2024, 9, 17045−17053

Table 5. Games−Howell Pairwise Comparison between the Negative Control Assays Using A-PCL and R-PCL Meshes and Their CaOx EC with Three Concentrations of ZP

sample	n	$\bar{x}$	grouping							
CN-R	38	**15.70**	A	B						
BC	172	12.965		B						
ZP-A 1 mg/L	46	8,644			C					
CN-A	108	7.933			C	D	E			
ZP-R 1 g/L	227	6,770				D				
ZP-R 5 g/L	199	6,193				D	E			
ZP-R 1 mg/L	148	*4,414*						F	G	
ZP-A 1 g/L	220	*3,973*						F	G	
ZP-A 5 g/L	272	*3,898*							G	

difference in the values of n in the EC test in the presence of ZP additive only when 1 mg/L ZP was used. The smallest size crystals are obtained with 1 mg/L ZP and the largest crystals are obtained with the R-PCL without ZP. It can be seen that the effect of increasing the concentration of ZP in the experimental CaOx EC condition is again significant in the results of n obtained. Table 5 summarizes the overall comparison in all CaOx EC and analyzed by "Games−Howell" pairwise comparison in a single comparison to evaluate the effect of ZP in EC assays at the three concentrations is independent of the type of mesh used.

The results for the lowest and highest median values are shown in italics and bold, respectively. Medians that do not share a letter indicate that they are significantly different.

The Games−Howell method also showed a statistical difference between the average number of crystal size ($\bar{x}$), i.e., the EC assays of CaOx on different types of meshes and the concentrations of ZP were significant, reflecting its effect on the variation of n values, and that the largest and smallest crystal sizes were obtained with the A-PCL meshes with ZP at 1 mg/L and 5 g/L, respectively.

The results of all of the EC CaOx assays were also analyzed in an ordinal way, considering the total number of crystals (N) and the sample size (n), in an attempt to know the influence in each experimental condition (Table 6). This analysis allows to cross the information obtained with the ZP as additive and to know precisely the effect of ZP to modulate N and n compared to control assays and to understand the effect of ZP on a EPM meshes involved in the CaOx kidney stone process, which is a frequent pathological condition in mammals. With regard to the N values, the CN-R control and the use of ZP-A at 1 mg/L reached positions 1 and 2, respectively. In general, when the ZP was used at the lowest concentration, the CN-R and CN-A controls had the lower numbers 1 to 4, whereas ZP-A at 5 g/L had the highest N value, placing it in the highest position.

Table 6. Ordinal Comparison of the Total Number of CaOx Crystals and the Average Crystal Size in Each EC Experiment with the Control Assay Without PCL Mesh (BC), with CN-A and CN-R Meshes, and with ZP-A and ZP-R at Concentrations of 1, 1, and 5 g/L, Respectively

sample	total number of crystals (N)	sample size (n)
CN-R	1°	9°
ZP-A 1 mg/L	2°	7°
CN-A	3°	6°
ZP-R 1 mg/L	4°	3°
BC	5°	8°
ZPD 5 g/L	6°	4°
ZP-A 1 g/L	7°	2°
ZP-R 1 g/L	8°	5°
ZP-A 5 g/L	9°	1°

The 1° value represents the lowest N and n values in each CaOx EC assay.

When comparing all EC assays, CN-R and ZP-A at 5 g/L, having the lowest and highest N values, corresponded inversely to the sample sizes (n). In fact, the CN-R and ZP-A at 5 g/L were ranked the ninth and first places, respectively. On the other hand, ZP-A and ZP-R had the largest n value at 1 mg/L, ranking seventh and fifth, respectively, when comparing all EC assays using A-PCL and R-PCL with ZP additive.

In general, experimental conditions using CN-R and CN-A without ZP and negative control experiments (BC) had high n values showing the ninth, sixth, and eighth places, respectively. Also, the EC assay with ZP-A with high ZP concentrations (5 and 1 g/L), showing the highest N value (ninth and seventh places), were ranked first and second with respect to sample size (n), indicating its improved positioning. Therefore, we have shown that there were significant differences in all the in vitro CaOx EC assays, either in the BC, with CN-A and CN-R meshes, or in the presence of ZP-A and ZP-R meshes at 1, 1, and 5 g/L, respectively. The above shows a very radical variation between the EC assays using PCL at different ZP concentrations, which can be considered an improved experimental condition compared to the control as summarized in Table 5.

OM analysis readily revealed the presence of crystals on the ITO glass, and SEM showed in more detail the morphologies of COD and COM and the distribution of the PCL fibers of the PCL-EPM used in the in vitro CaOx EC. EDS identified the Ca, C, and O atoms from the CaOx, elements from the PCL, and a variety of other elements from the ITO glass and ZP additive.

XRD analysis revealed a COM phase in the control EC assays. However, a clear predominance of the COD phase was observed in the EC assays of A-PCL and R-PCL without ZP (Figure S3). When the CaOx EC was performed on the ZP-loaded PCL meshes, the XRD results indicated that the presence of ZP and its concentration controlled the number and the intensity of the crystallographic peaks in both PCL-EPM systems, and in the case of R-PCL at 5 g/L, a higher proportion of the COD phase was found. We believe that the natural extract with abundant presence of extra ions can influence the interaction of Ca^{2+} and oxalate ions, modifying the nucleation on the local surface of the PCL-EPM, giving rise to a heterogeneous nucleation control, inhibiting the mechanism of COM and promoting the formation of COD

https://doi.org/10.1021/acsomega.3c08736
ACS Omega 2024, 9, 17045−17053

crystals. The effect of metal ions on the crystallization growth rate of inorganic minerals has been reported. For example, Mg ions do not incorporate into the COM crystal, but they do alter the crystal surface and affect the atomic interaction of COM and COD, as well as the interaction of CaOx crystals with cellular proteins. These findings provide new insights into the mechanisms of pathological nephrolithiasis.[28,29] Therefore, the specific inhibitory role of ZP may be attributed to its selective attachment of ZP to the (−101) plane of the CaOx crystals. This binding prevents the aggregation of COM and the formation of kidney stones, acting as a regulator of pathological biomineralization. It is known that the Mg element can form complexes with oxalate ions and reduce local supersaturation, thereby acting as an inhibitor of CaOx stone formation.[30]

CP technique revealed small voltage variations during the EC assays when the ITO glass (control experiments) and PCL-EPM systems were without ZP additive. However, the chronopotentiometric analysis of the EC assays performed on ITO modified with PCL-EPM and ZP showed a concentration-dependent relationship. The potential (V) increased from 2.5 to 10 V using lower to higher concentrations of ZP, and the onset of crystalline deposition of CaOx was also affected. This demonstrates a modulatory effect of the promoter−inhibitor that depends on the PCL-EPM and the concentration of ZP. Our findings agree with the effect of both PCL-EPM systems at the three ZP concentrations (Table 6). Even at low concentrations of ZP, its presence and its effect on the modulation and stabilization of healthy COD were demonstrated by EDS and XRD, respectively.

4. CONCLUSIONS

PCL-EPM loaded with ZP were fabricated directly on the ITO glass and used as a 3D template for in vitro EC of CaOx. During the EC experiments, ZP controlled the total number of crystals (N) and reduced the sample size (n) of CaOx, resulting in the stabilization of the COD phase with a bipyramidal morphology. Interestingly, ZP prevented the formation of the (−101) plane in the COM crystals. The antilithiatic activity of ZP is fully consistent with the increase in the applied voltage registered in the CP measurements, in which we found concentration-dependent kinetics of the ZP additive on the EC of CaOx. In conclusion, the most effective experimental condition of CaOx EC with PCL-EPM was by using ZP at the highest concentration in ZPA-PCL and R-PCL, obtaining a significant reduction in the sample size (n) of CaOx, stabilization of the COD form, and the absence of the crystallographic diffraction plane (−101) associated with the pathological COM crystals.

■ ASSOCIATED CONTENT

Supporting Information

The Supporting Information is available free of charge at https://pubs.acs.org/doi/10.1021/acsomega.3c08736.

OM images of CaOx obtained via EC on ITO modified with PCL fibers of (a) control (base ITO), (b) A-PCL, and (c) R-PCL; OM images of CaOx obtained via EC on ITO modified with PCL fibers in the presence of ZP additive: (a) A-PCL with 1 mg/L ZP, (b) A-PCL with 1 g/L ZP, (c) A-PCL with 5 g/L ZP, (d) R-PCL with 1 mg/L ZP, (e) R-PCL with 1 g/L ZP, and (f) R-PCL with 5 g/L ZP; XRD of CaOx obtained on ITO modified with PCL fibers and ZP additive: (a) ITO substrate, (b) control (without PCL fibers), (c) A-PCL and (d) R-PCL; determination of the total number of CaOx crystals, number estimation (crystal numbers/mm^2), average number of CaOx crystal, size of crystals, confidence interval and statistical considerations in the CaOx EC assays using Minitab 19; normality test (Anderson−Darling). report summaries. (a) 1 BC, (b) 2 CN-A, (c) CN-R, (d) ZP-A 1 mg/L, (e) ZP-R 1 mg/L, (f) ZP-A 1 g/L, (g) ZP-R 1 g/L, (h) ZP-A 5 g/L, and (i) ZP-R 5 g/L; equality of variances test (Bonferroni−Levene). test of equality of variances: (1) BC, (2) CN-A, (3) CN-R, (4) ZP-A 1 mg/L, (5) ZP-R 1 mg/L, (6) ZP-A 1g/L, (7) ZP-R 1g/L and (8) ZP-R 5 g/L; Welch's test—paired comparison Games−Howell. analysis a−c (PDF)

■ AUTHOR INFORMATION

Corresponding Author

Andrónico Neira-Carrillo − *Department of Biological and Animal Science, Faculty of Veterinary and Animal Sciences, Universidad de Chile, Santiago 1025000, Chile;* orcid.org/0000-0003-0060-7518; Email: aneira@uchile.cl

Authors

Tatiana Zegers Arce − *Department of Biological and Animal Science, Faculty of Veterinary and Animal Sciences, Universidad de Chile, Santiago 1025000, Chile*

Mehrdad Yazdani-Pedram − *Department of Organic and Physical Chemistry, Faculty of Chemical and Pharmaceutical Sciences, Universidad de Chile, Santiago 8380492, Chile*

Complete contact information is available at: https://pubs.acs.org/10.1021/acsomega.3c08736

Author Contributions

The manuscript was written through contributions of all authors. All authors have given approval to the final version of the manuscript.

Funding

Funding: This work was supported by the Ministry of Science and Technology through the Chilean Agency for Research and Development (ANID), Project FONDECYT 1 211 345, Chile.

Notes

The authors declare no competing financial interest.

■ ACKNOWLEDGMENTS

This work was supported by FONDECYT No 1211345 granted by the Chilean Agency for Research and Development (ANID).

■ REFERENCES

(1) Lowenstam, H. A. W.; Weiner, S. *On Biomineralization*; Oxford University Press: New York; 1989.

(2) Estroff, L. A. Introduction: Biomineralization. *Chem. Rev.* **2008**, *108*, 4329−4331.

(3) Simkiss, K.; Wilbur, K. M. *Biomineralization: cell biology and mineral deposition*; Academic Press: San Diego, 1989; p 337.

(4) Mann, S. *Biomineralization Principles and concepts in bioinorganic materials chemistry*; Oxford University Press, 2001.

(5) Arias, J. L.; Fernández, M. S. Biomimetic processes through the study of mineralized shells. *Mater. Charact.* **2003**, *50*, 189−195.

(6) Wesson, J. A.; Ward, M. D. Pathological Biomineralization of Kidney Stones. *Elements* **2007**, *3* (6), 415−421.
(7) Daudon, M.; Bazin, D.; Letavernier, E. Randall's plaque as the origin of calcium oxalate kidney stones. *Urolithiasis* **2015**, *43*, 5−11.
(8) Xu, S.; Cao, D.; Liu, Y.; Wang, Y. Role of Additives in Crystal Nucleation from Solutions: A Review. *Cryst. Growth Des.* **2022**, *22*, 2001−2022.
(9) Zhang, Y.-H.; Li, C.-Y.; Zou, G.-J.; Xian, J.-Y.; Zhang, Q.; Yu, B.-X.; Huang, L.-H.; Liu, H.-X.; Sun, X.-Y. Corn silk polysaccharides with different carboxyl contents reduce the oxidative damage of renal epithelial cells by inhibiting endocytosis of nano-calcium oxalate crystals. *ACS Omega* **2023**, *8*, 25839−25849.
(10) Chen, J.-Y.; Sun, X.-Y.; Ouyang, J.-M. Modulation of calcium oxalate crystal growth and protection from oxidatively damaged renal epithelial cells of corn silk polysaccharides with different molecular weights. *Oxid. Med. Cell. Longev.* **2020**, *2020*, 6982948.
(11) Kant, R.; Singh, T. G.; Singh, S. Mechanistic approach to herbal formulations used for urolithiasis treatment. *Obes. Med.* **2020**, *19*, 100266.
(12) El Habbani, R.; Lahrichi, A.; Houssaini, T. S.; Kachkoul, R.; Mohim, M.; Chouhani, B. A.; Chaqroune, A. In vitro mass reduction of calcium oxalate urinary calculi by some medicinal plants. *Afr. J. Urol.* **2021**, *27*, 28.
(13) Kaviraj, M.; Andrew Pradeep, M.; Satheesh, D. In-vitro investigation on antiurolithiatic activity and phytochemical examination of Aerva lanata and bryophyllum pinnatum: A comparative study. *J. Indian Chem. Soc.* **2022**, *99*, 100487.
(14) Menon, S.; Al-Saadi, A. S.; Al-Aamri, N. J.; Al-Jaradi, A.-Z. H.; Al Mamari, H. K.; Al Haddabi, L. H.; Jayachandran, V. P.; Shinisha, C. B. Inhibition of crystallization of calcium oxalate monohydrate using leaves from different species of Moringa − Experimental and theoretical studies. *J. Cryst. Growth* **2022**, *598*, 126859.
(15) Bawari, S.; Sah, A. N.; Gupta, P.; Zengin, G.; Tewari, D. Himalayan Citrus jambhiri juice reduced renal crystallization in nephrolithiasis by possible inhibition of glycolate oxidase and matrix metalloproteinases. *J. Ethnopharmacol.* **2023**, *306*, 11615.
(16) Rashid, S.; Sameti, M.; Alqarni, M. H. In vivo investigation of the inhibitory effect of Peganum harmala L. and its major alkaloids on ethylene glycol-induced urolithiasis in rats. *J. Ethnopharmacol.* **2023**, *300*, 115752.
(17) Neira-Carrillo, A.; Vásquez-Quitral, P.; Sánchez, M.; Vargas-Fernández, A.; Silva, J. F. Control of calcium oxalate morphology through electrocrystallization as an electrochemical approach for preventing pathological disease. *Ionics* **2015**, *21*, 3141−3149.
(18) Ruiz-Agudo, E.; Burgos-Cara, A.; Ruiz-Agudo, C.; Ibañez-Velasco, A.; Cölfen, H.; Rodriguez-Navarro, C. A non-classical view on calcium oxalate precipitation and the role of citrate. *Nat. Commun.* **2017**, *8*, 768.
(19) Sun, X. Y.; Ouyang, J. M.; Xu, M. Synthesis, characterization, and cytotoxicity assay of calcium oxalate dihydrate crystals in various shapes. *CrystEngcomm* **2016**, *18*, 5463−5473.
(20) Mittal, A.; Tandon, S.; Singla, S. K.; Tandon, C. International in vitro studies reveal antiurolithic effect of terminalia arjuna using quantitative morphological information from computerized microscopy. *Int. Braz J. Urol.* **2015**, *41*, 935−944.
(21) Butto, N.; Vera, N. C.; Díaz-Soler, F.; Yazdani-Pedram, M.; Neira-Carrillo, A. Effect of chitosan electrospun fiber mesh as template on the crystallization of calcium oxalate. *Crystals* **2020**, *10* (6), 453.
(22) Butto-Miranda, N.; Cabrera-Barjas, G.; Ibáñez, A.; Neira-Carrillo, A. Preparation of novel electrospun organic−inorganic hybrid nanofibers based on polycaprolactone, glycine betaine, and calcium carbonate (P/G/CaCO3-EPnF). *Crystals* **2023**, *13*, 611.
(23) Weis, A. Mineralization in organic matrix frameworks. *Rev. Miner. Geochem.* **2003**, *54* (1), 249−289.
(24) Arce, T. Z.; Yazdani-Pedram, M.; Neira-Carrillo, A. Andrónico Neira-Carrillo. Electrocrystallization of calcium oxalate on electrospun PCL fibers loaded with phytic acid as a template. *Polymers* **2022**, *14*, 3190.
(25) Ketrane, R.; Saidani, B.; Gil, O.; Leleyter, L.; Baraud, F. Efficiency of five scale inhibitors on calcium carbonate precipitation from hard water: Effect of temperature and concentration. *Desalination* **2009**, *249*, 1397−1404.
(26) Rugna, A. Z.; Vugin, A.; Gurni, A. A.; Wagner, M. L. Marcha fitoquímica comparativa entre las hojas y los rizomas de Smilax campestris Griseb. − Smilacaceae. *Dominguezia* **2003**, *19* (1), 25−29.
(27) Guambo Delgado, D. M. Identificación de los metabolitos secundarios de la raíz de zarzaparrilla (Smilax aspera), para la elaboración de una bebida BSc thesis in Agroindustrial Engineering; Univeridad Nacional de Chimborazo, Facultad de Ingeniería Agro-industrial: Riobamba, Ecuador, 2016
(28) Lieske, J. C.; Farell, G.; Deganello, S. The effect of ions at the surface of calcium oxalate monohydrate crystals on cell-crystal interactions. *Urol. Res.* **2004**, *32* (2), 117−123.
(29) Alamani, B. G.; Gale, J. D.; Rimer, J. D. Zinc ions modify calcium oxalate growth by distinct transformation of crystal surface termination. *Cryst. Growth Des.* **2021**, *21*, 3375−3383.
(30) Basavaraj, D. R.; Biyani, C. S.; Browning, A. J.; Cartledge, J. J. The role of urinary kidney stone inhibitors and promoters in the pathogenesis of calcium containing renal stones. *EAU-EBU Update Series* **2007**, *5* (3), 126−136.

https://doi.org/10.1021/acsomega.3c08736
ACS Omega 2024, 9, 17045−17053